Available online at www.sciencedirect.com

ScienceDirect

Acta Materialia 56 (2008) 1151–1164

Acta MATERIALIA

www.elsevier.com/locate/actamat

Effect of a finite quadruple junction mobility on grain microstructure evolution: Theory and simulation

L.A. Barrales Mora [a,*], V. Mohles [a], L.S. Shvindlerman [a,b], G. Gottstein [a]

[a] *Institut für Metallkunde und Metallphysik, RWTH Aachen, Kopernikusstrasse 14, D-52056 Aachen, Germany*
[b] *Institute of Solid State Physics, Russian Academy of Sciences, Chernogolovka, Moscow District 142432, Russia*

Received 15 August 2007; received in revised form 6 November 2007; accepted 11 November 2007

Abstract

The effect of a finite quadruple junction mobility on grain growth evolution has been studied by means of computer simulations. For this purpose a special three-dimensional grain assembly is proposed, which permits a steady-state motion of the grain boundaries and junctions of the system. It was found that the behavior of the system is determined by the dimensionless parameter Λ_{qp}, which is related to the quadruple junction mobility. Numerous simulations were carried out in order to determine the effect of this parameter on grain growth. The results show that a finite quadruple junction mobility can slow down grain growth. However, the simulations also demonstrated that a finite triple line mobility hinders grain growth even more effectively.

Keywords: Grain growth; Modeling; Theory; Simulation; Grain-boundary migration

1. Introduction

A polycrystalline aggregate is a system composed of grains, grain boundaries, triple lines and quadruple junctions. This system forms a topological network with a specific number of elements. For a long time, it was assumed that the only element affecting grain-boundary migration was the grain-boundary itself. Triple lines and quadruple junctions were not taken into account because these elements were believed not to drag grain-boundary motion. However, in recent years several theoretical and experimental studies [1–3] have demonstrated that triple lines can have kinetics different from the adjoining grain boundaries, i.e. triple lines can possess a finite mobility, and therefore can drag grain-boundary motion. The first experimental investigations were conducted only in a narrow range of geometrical configurations which allow a steady-state motion of a system of connected boundaries [4]. Later on, experimental and theoretical investigations on polycrystalline samples indeed confirmed the dragging effect of triple lines [5].

Whereas the experimental study of triple lines can be easily conducted in quasi-two-dimensional systems, quadruple junctions are true three-dimensional features and hence their study can be only accomplished in three-dimensional space which is difficult to do by experiments on metals, since metals are opaque. As a first attempt to address this problem, Gottstein and Shvindlerman [6] introduced a new concept, which would permit the study of a finite quadruple junction mobility in a special grain assembly. In the current study, we extend this concept and explore the effect of a finite quadruple junction mobility on grain growth by means of computer simulations.

2. Grain-boundary junctions

The structural elements of a polycrystal are the grain boundaries, the triple lines and the quadruple junctions. A triple line is the region where three grain boundaries meet and interact with each other. Correspondingly, a

* Corresponding author. Tel.: +49 (0) 2418026877; fax: +49 (0) 2418022301.
E-mail address: barrales@imm.rwth-aachen.de (L.A. Barrales Mora).

1359-6454/$30.00
doi:10.1016/j.actamat.2007.11.013

quadruple junction is the point of intersection of four triple lines and respectively six grain boundaries. The evolution of such systems is determined by grain-boundary migration. However, triple lines and quadruple points may influence the evolution of the system as well.

2.1. Triple line effect on the evolution of connected grain-boundary systems

Shvindlerman et al. [7] were the first to consider the effect of triple lines on grain-boundary migration. They used a two-dimensional tri-crystalline system for the determination of the dimensionless parameter Λ_{tl} that characterizes the influence of a finite triple line mobility m_{tl} on the evolution of the system[1] and is given by

$$\Lambda_{tl} = \frac{m_{tl} \cdot r}{m_{gb}} \tag{1}$$

where m_{gb} is the grain-boundary mobility and r represents the grain size. If $\Lambda_{tl} \ll 1$, the triple line mobility governs the motion of the boundary system. Conversely, if $\Lambda_{tl} \gg 1$ the evolution of the system is determined by the grain-boundary mobility [4].

2.2. Quadruple junction effect on the evolution of connected grain-boundary systems

In analogy with triple lines, it can be envisaged that also quadruple junctions can drag the evolution of connected systems. In fact, Gottstein and Shvindlerman [6] proposed the four grains assembly outlined in Fig. 1. The main feature of this configuration is that one of the four grains has only three boundaries as depicted by the enclosing triple lines shown in Fig. 1. In such configuration, it is assumed that the motion of the triple lines in the system proceeds under the action of the triple line tension γ^{l} and is assumed to occur in steady-state (which takes place if the shrinkage of the three-sided cross-section proceeds much more slowly than the displacement of the quadruple junction). The dimensionless parameter describing the influence of the quadruple junction is given by

$$\Lambda_{qp} = \frac{m_{qp} \cdot a}{m_{tl}} = \frac{2\theta_1}{2\cos\theta_1 - 1} \tag{2}$$

where m_{qp} is the quadruple junction mobility, m_{tl} is the triple line mobility, θ_1 is the angle at the tip of the triple lines at the quadruple junction, and a is the grain size (Fig. 1). Obviously, the effect of a finite quadruple junction mobility is reflected by the change of the angle θ_1. For a perfectly mobile quadruple junction $\Lambda_{qp} \to \infty$ and $\theta_1 \to \pi/3$, whereas when the quadruple junction strongly drags the motion of the system, $\Lambda_{qp} \to 0$ and $\theta_1 \to 0$.

[1] As the considered system is two-dimensional, the mobility originally regarded was that of the triple junction. A triple junction is normally considered as the point that forms when a triple line intersects a plane. However, the mobility is a property of the line and thus does not depend on the dimensionality of the space in which this defect is represented. For the sake of clarity, in this paper, we will refer exclusively to these defects and their properties in their three-dimensional configuration.

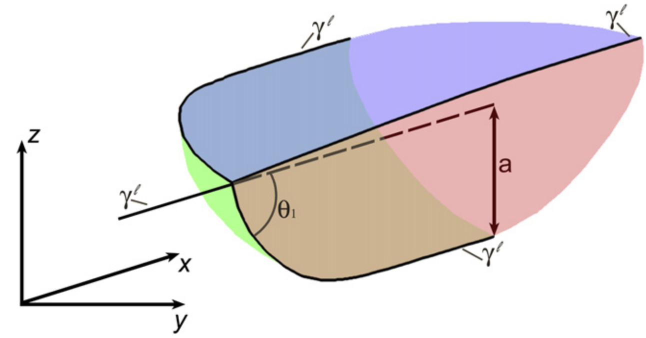

Fig. 1. Grain assembly proposed in Ref. [6] for the determination of the dimensionless parameter Λ_{qp}.

The assumptions made for the derivation of Eq. (2) imply that the triple lines move under the action of their own line tension, but that does not mean that this driving force exclusively produces the motion of the system. In fact, the main driving force stems from grain-boundary curvature. The concomitant movement of the elements entails an adaptation of the driving forces to the lowest kinetics. For instance, if the quadruple junction drags the motion of the system, the curvature of the triple lines and grain boundaries needs to adjust in order to lower the driving force. The implications of a finite mobility of the different structural elements can be only analyzed in an objective frame, which is given by Eqs. (1) and (2). Since the mobility of the grain boundaries is finite, it is also reasonable to express Λ_{qp} in terms of m_{gb} [1]

$$\Lambda_{qp} = \frac{m_{qp} \cdot a^2}{m_{gb}} \tag{3}$$

3. Effect of a finite quadruple junction mobility on the evolution of the four grains assembly

For the simulations, a three-dimensional vertex model was used. The model is detailed in Appendix A. The geometry of the three-sided grain used in the simulations is shown in Fig. 2; it perfectly matches the configuration shown in Fig. 1. As stated in a previous section, the shrinkage of the cross-section should not contribute to the volume change of the grain, in order to maintain the geometry for the displacement of the quadruple junctions. To check the validity of this assumption, the computed net displacements of the triple line in the z-direction and the quadruple junction in x-direction are plotted in Fig. 3a for the case of an infinite quadruple junction mobility m_{qp}. Contrary to expectations, the magnitude of the triple line displacement is not negligible. The velocity of both junction elements is not very different (Fig. 3b); the triple line velocity is only approximately 3–4 times slower than the quadruple junction velocity. In fact, if the three-sided grain is very long (a prerequisite for Eq. (2)), the

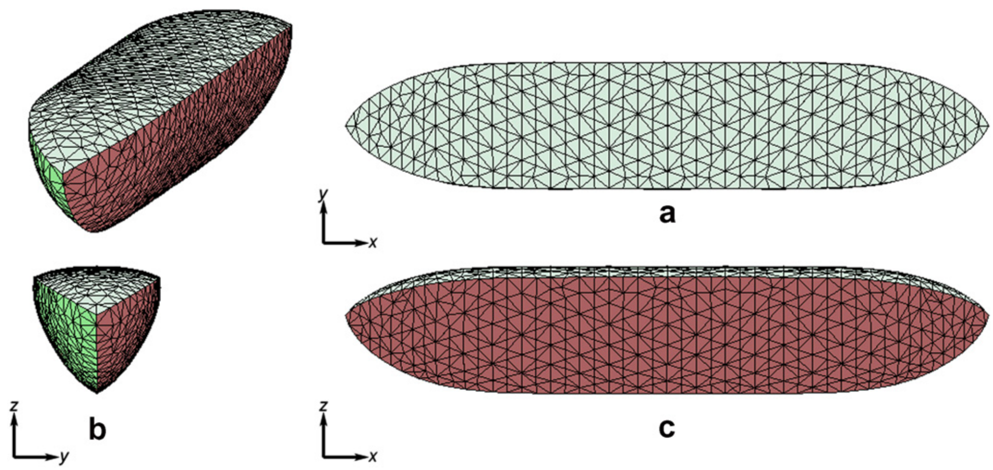

Fig. 2. Geometry of the three-sided grain shown in Fig. 1: (a) top view, (b) front view and (c) lateral view.

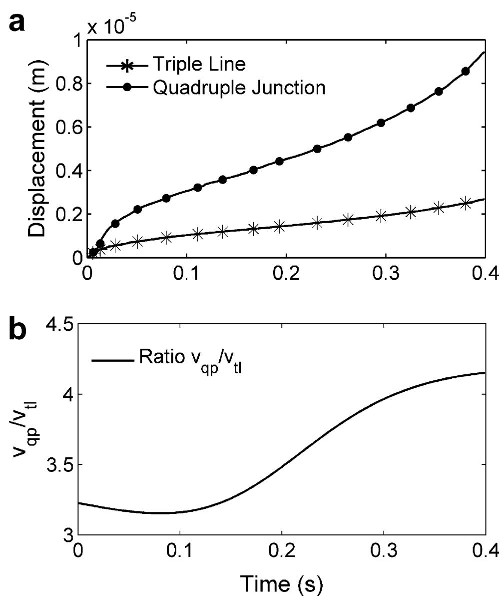

Fig. 3. Triple line and quadruple junction displacement in the x- and z-directions, respectively (a); ratio of quadruple junction to triple line velocity (b).

cross-section and hence the whole grain vanishes even before the two quadruple points meet. The necessary condition that the motion of the quadruple junction essentially dominates the volume change – if the shrinkage of the cross section cannot be avoided – can only be achieved for very small Λ_{tl}, when the shrinkage of the cross section is dominated by triple line kinetics. In this case the grain boundaries are virtually flat (causing a reduction of the net driving force for the shrinkage of the cross section). However, this would severely restrict the kinetic range where the investigation can be carried out.

4. Steady-state quadruple junction motion

The cross section of the previous configuration corresponds to a three-sided grain, which is subject to a high shrinking rate. By contrast, for a steady-state quadruple junction motion a cross-section, which neither grows nor shrinks, is needed. The von Neumann–Mullins law [8] predicts that only a grain with a six-sided cross section can fulfill this condition. Furthermore, to make sure that the dihedral angle between adjacent boundaries remains 120° is necessary that the system consists only of regular hexagons (Fig. 4a), i.e. the cross section plane should be filled by regular hexagons. The corresponding three-dimensional grain assembly is an arrangement of hexagonal prisms (Fig. 4b). It is noted that in the front and the back of the hexagonal prisms two more grains are connected to the system, in order to generate intergranular quadruple junctions.

4.1. Equations of motion

As in the configuration shown in Fig. 1, the motion proceeds under the action of the triple junction line tension γ^{l}, which can be negative or positive. Fig. 5a shows two grains of the configuration as well as the grain boundaries meeting at a quadruple junction. The condition for steady-state motion of the system is that the line tensions of all triple lines at the quadruple junction have the same sign. Configurations, which are formed by triple lines with line tension of different sign, are possible as well; however, configurations with steady-state motion are unlikely to exist.

From Fig. 5a it is possible to extract the geometry of the triple lines meeting at their point of intersection. The forces acting on the quadruple junction due to the triple junction line tensions are depicted in Fig. 5b. θ denotes the angle between adjacent triple lines on the same grain-boundary. The force P acting on the quadruple junction can be determined from the sum over the line tension of all triple lines meeting at the quadruple junction

$$\vec{P} = \vec{F}_1 + \vec{F}_2 + \vec{F}_3 + \vec{F}_4 \tag{4}$$

For the used geometry, the sum is reduced to the sum of the components in x-direction of the line tension γ^{l}. Due

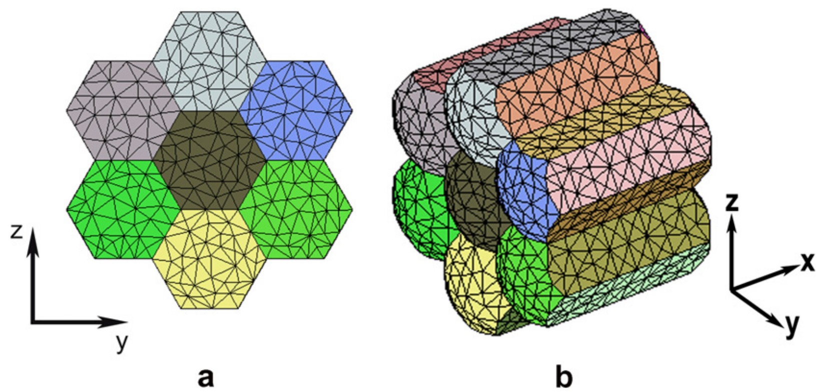

Fig. 4. (a) Cross section of the used grain assembly, it is composed of regular hexagons and the dihedral angles are 120°. For this reason, no shrinkage or growth of the cross section occurs; (b) the special grain assembly allows a steady-state motion of the quadruple points. Only the first layer of grains adjoining the central grain is shown, however, there are more hexagonal grains filling the space (plane y–z) while in the x-direction, in front and in the back of the configuration, two more grains, whose shape is irrelevant, adjoin the hexagonal grains.

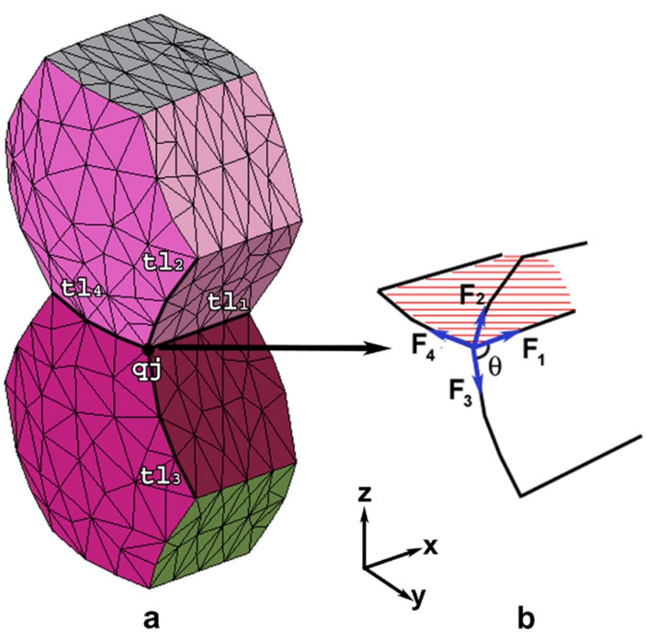

Fig. 5. Geometry of four triple lines (tl) meeting at the quadruple junction (qj).

to the symmetry of forces at the quadruple junction the sum of forces in the y- and z-directions, respectively, are zero. Hence,

$$P = \gamma^{l}(1 + 3\cos\theta) \tag{5}$$

Then, the velocity of the quadruple junction reads

$$v_{qp} = m_{qp}P = m_{qp}\gamma^{l}(1 + 3\cos\theta) \tag{6}$$

The equilibrium angle at zero force on the quadruple point is easily calculated. It corresponds to the tetrahedral dihedral angle $\theta_\infty = \arccos(-1/3) \approx 109.47°$.

Taking into account the shape of the grain boundaries, the problem can be comprehensively described. In Fig. 6 the grain-boundary shaded in Fig. 5b is shown with a new coordinate system. The variables used for the derivation of the equation of motion are also shown.

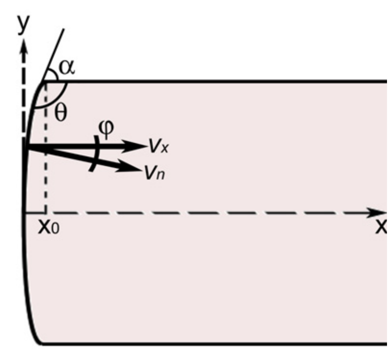

Fig. 6. Shape of the grain boundaries and definition of the variables used for the derivation of the equation of motion.

The velocity of a moving triple line is assumed to be given by

$$v_n = m_{tl}\gamma^{l}\kappa \tag{7}$$

where

$$\kappa = -y''[1 + (y')^2]^{-3/2} \tag{8}$$

represents the curvature of the triple line. The horizontal steady-state velocity v_x of the system is related to the normal velocity v_n as follows:

$$v_n = v_x\cos\varphi = v_x\frac{y'}{(1 + (y')^2)^{1/2}} \tag{9}$$

Combining Eqs. (7)–(9) yields the differential equation

$$y'' = -\frac{v_x}{m_{tl}\gamma^{l}}y'[1 + (y')^2] \tag{10}$$

which needs to be solved under the boundary conditions $y(0) = 0$, $y'(x_0) = \tan\alpha$, $y'(0) = \infty$, and $\alpha = \pi - \theta$.

The length x_0 and the angle α are clear from Fig. 6, $y(x)$ is the shape of the triple line obtained by integration of Eq. (10) and given by

$$y(x) = -\frac{x_0}{\ln\sin\alpha}\arccos\left[e^{\left(\frac{x}{x_0}\right)\ln\sin\alpha}\right] \tag{11}$$

Finally, the velocity v_x of steady-state motion of the triple line is equal to

$$v_x = -\frac{m_{tl}\gamma^l}{x_0}\ln\sin\alpha \tag{12}$$

Since v_x (Eq. (12)) and v_{qp} (Eq. (6)) have to be identical, this defines the dimensionless parameter Λ_{qp} which characterizes the influence of a finite quadruple junction mobility on grain-boundary migration.

$$-\frac{m_{tl}\gamma^l}{x_0}\ln\sin\alpha = m_{qp}\gamma^l[1+3\cos\theta] \tag{13}$$

$$\frac{m_{qp}\cdot x_0}{m_{tl}} = \Lambda_{qp} = -\frac{\ln\sin\alpha}{1+3\cos\theta} \tag{14}$$

Substituting α by θ we obtain the final expression in terms of this angle

$$\Lambda_{qp} = -\frac{\ln\sin(\pi-\theta)}{1+3\cos\theta} = -\frac{\ln\sin\theta}{1+3\cos\theta} = \frac{m_{qp}\cdot x_0}{m_{tl}} \tag{15}$$

If the quadruple junction is perfectly mobile, then $\Lambda_{qp}\to\infty$ and $\theta\to 109.47°$, which is the equilibrium angle. In contrast, if the quadruple junction moves slowly and drags the migration of the triple lines then $\Lambda_{qp}\to 0$ and $\theta\to\pi/2$.

4.2. Effect on grain microstructure evolution

From Eq. (15), it is clear that the angle θ is completely defined by the dimensionless parameter Λ_{qp}, which, in turn, does not only depend on the triple line and quadruple junction mobilities but also on the grain size, x_0. It is noted that the term x_0 is not the grain size itself but is directly related to it. This is relevant because it indicates that, as in the case of triple line drag, the effect of quadruple junctions increases with decreasing grain size.

In order to demonstrate that the motion of the configuration attains a steady-state motion, two simulations under extreme conditions were performed. For the first simulation triple line and quadruple junction mobilities were considered infinite. By contrast, for the second simulation an extremely low quadruple junction mobility was used ($\Lambda_{qp} = 1.2\times10^{-3}$).

Fig. 7 shows the longitudinal displacements of the grain-boundary and the quadruple junction as a function of time for the first case ($\Lambda_{tl}=\infty$, $\Lambda_{qp}=\infty$). The displacement was taken directly from the simulations. Initially, all the boundaries were flat; after a short time the boundaries became curved and the motion proceeded in steady-state. Minor jitters are only the artifacts of the simulations. The displacement of both considered elements is linear with time, the velocities of grain-boundary and the quadruple junction are practically the same, i.e. both lines have the same slope.

As expected, the motion also proceeds in steady-state when Λ_{qp} is very low, as shown in Fig. 8. The displacement is also linear in time, and both velocities are almost equal. Evidently, the proposed grain configuration also attains a steady-state behavior in the course of time.

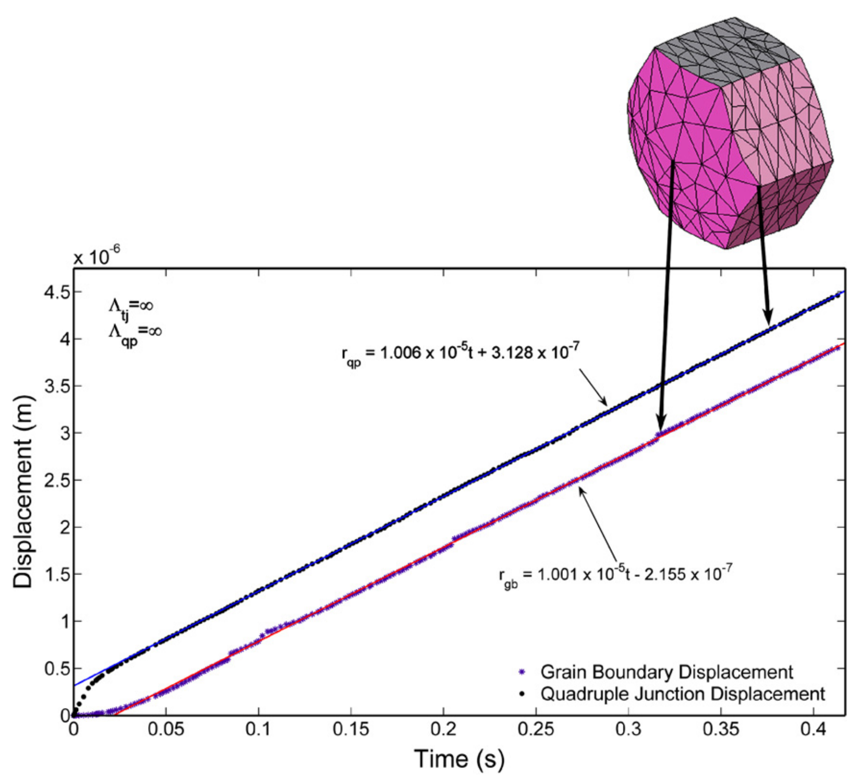

Fig. 7. Displacement of grain-boundary and quadruple junction vs. time. The triple line and quadruple junction mobilities were considered to be infinite. The solid lines are linear fits and indicate the steady-state motion of the configuration since they are practically parallel. The grain indicates the points where the displacements were taken from.

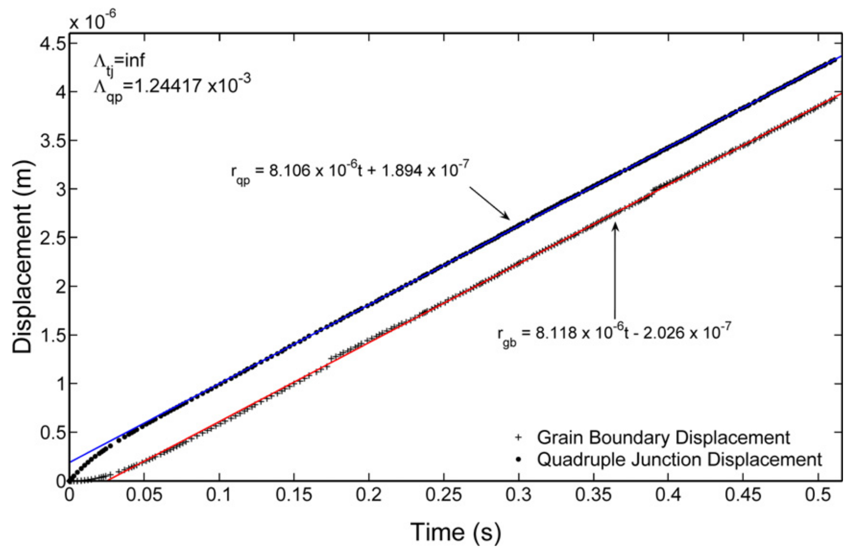

Fig. 8. Grain-boundary and quadruple junction displacement vs. time for very low quadruple junction mobility. Steady-state motion also occurs for this condition.

One effect of a finite quadruple junction mobility can be seen in the shape of the grain-boundary. The triple lines delimiting the boundary become flat as a result of the decrease of Λ_{qp} (Fig. 9). Eq. (15) predicts that the effect of Λ_{qp} is reflected by a change of the angle θ, however, this also impacts the curvature of the triple lines and hence the shape of the grain-boundary. The geometry of the triple lines in Fig. 9 was taken directly from the simulations. The steady-state angles obtained from the simulations agree very well with the theoretical curve (Eq. (15)), as shown in Fig. 10.

Qualitatively, a finite quadruple junction mobility can modify the geometry of the evolving configuration. However, for a quantitative description it is necessary to evaluate the grain size evolution as a function of Λ_{qp}. In Fig. 11, the grain volume as a function of time is shown for different values of Λ_{qp}. A small but evident retardation of the kinetics can be observed with decreasing Λ_{qp}. This becomes more obvious in Fig. 12, where the relative volume change rate $(\dot{V}/\dot{V}_\infty)$ is plotted ($\dot{V}_\infty$ is the volume change rate when $\Lambda_{qp} \to \infty$). Apparently, $(\dot{V}/\dot{V}_\infty) \to 1$ when $\Lambda_{qp} \to \infty$. By contrast, when $\Lambda_{qp} \to 0$, $(\dot{V}/\dot{V}_\infty)$ should approach zero. In Fig. 12, however, only a moderate decrease is to be seen, which indicates that the overall effect of the quadruple junctions on grain growth evolution is also moderate. The limit $\Lambda_{qp} \to 0$ is thus only expected for practically immobile quadruple junctions because the volume change rate is indirectly a function of θ, Λ_{qp}, or $\dot{V} = f(v_{qp}) = f(\theta(\Lambda_{qp}))$.

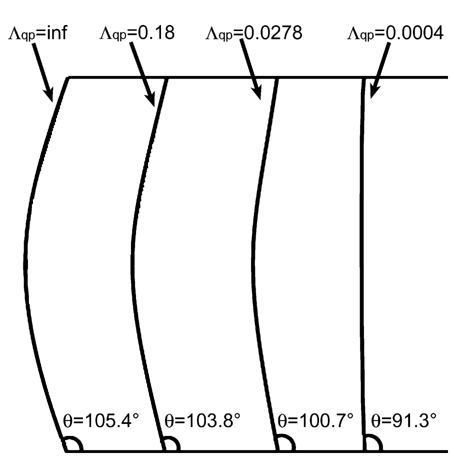

Fig. 9. Shape of the triple lines for different values of Λ_{qp}. Minor deviations from the theoretical angles can be attributed to the discretization used in the simulations.

Fig. 12 demonstrates the scaling behavior of the model. Three simulations with very different simulation parameters are compared. The first simulation assumed a certain value for the grain-boundary mobility, denoted as m_{gb0}, and an initial volume V_0 of the grains with hexagonal cross section of the configuration in Fig. 4. In a second simulation, the grain-boundary mobility was one order of magnitude lower than m_{gb0}, whereas a third simulation assumed a volume 1000 times larger than V_0. No significant differences in the relative volume change rate among the three conditions are found. Fig. 12b shows the same graph but restricted to the low and intermediate range of Λ_{qp}, for a more accurate comparison. The small variations of the different simulations are below the uncertainty range.

5. Effect of a finite triple line mobility on the evolution of the three-dimensional grain assembly

Due to the small size and the low frequency of quadruple junctions, it is expected that their effect on grain growth should be smaller in comparison, for example, to triple lines, which occupy a much larger volume and occur more frequently. In this section, the effect of triple lines on the kinetics of the same three-dimensional configuration will be briefly analyzed. In Fig. 13, the grain volume as a func-

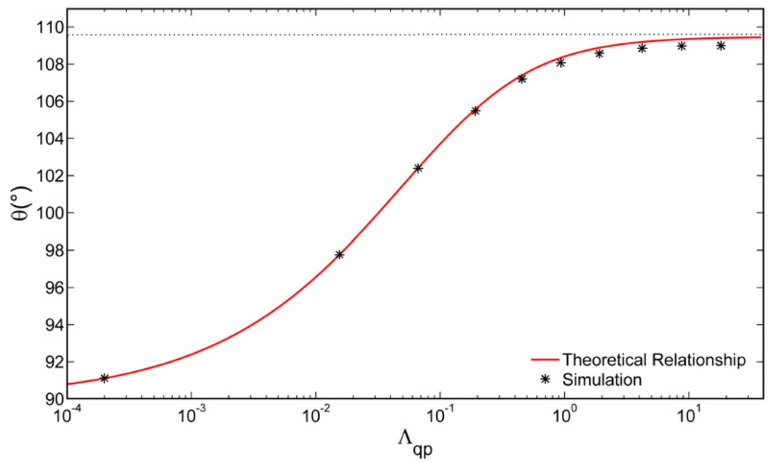

Fig. 10. Comparison of the function θ vs. $\Lambda_{\rm qp}$ and simulation results.

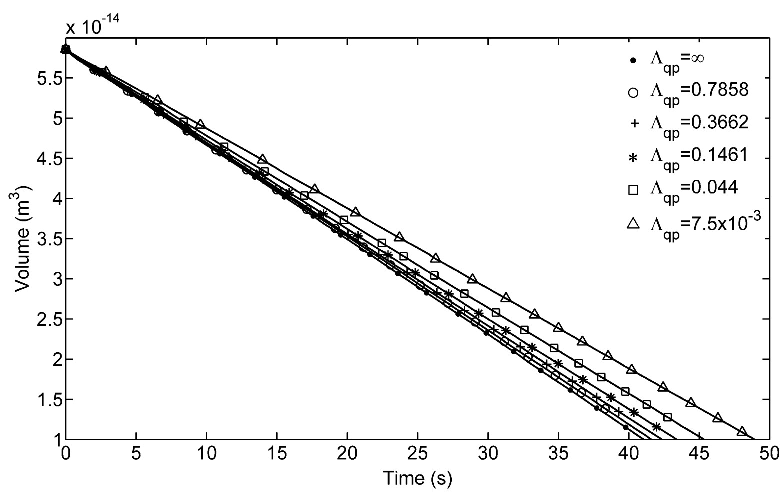

Fig. 11. Simulated grain volume vs. time for different $\Lambda_{\rm qp}$ (symbols are introduced along the lines for better identification).

tion of annealing time is presented. Here $m_{\rm qp}$ was considered infinite, while $m_{\rm tl}$ was varied to achieve different regimes of $\Lambda_{\rm tl}$. The retardation of the kinetics by a finite $m_{\rm tl}$ is evident. It can be observed that in the large and intermediate ranges ($\Lambda_{\rm tl} = [\infty, \sim 1]$) the volume decreases linearly with time. This means that the motion of the grain-boundary network occurs under steady-state conditions. However, for values of $\Lambda_{\rm tl} \ll 1$ the linearity is lost. Under such conditions the kinetics become triple line dominated, because the original curved grain boundaries become flat and the dihedral angles at triple lines deviate from the equilibrium angle (120°). At first glance, the effect of triple lines is more pronounced than the effect of quadruple junctions.

5.1. Triple line vs. quadruple junction drag

The comparison between triple line and quadruple junction kinetics serves to better understand the phenomenology of grain growth, especially in nanocrystalline materials. However, for the considered grain arrangement such comparison has to be restricted to the regime of large and intermediates values of $\Lambda_{\rm tl}$, because as shown in Fig. 13, for low values of $\Lambda_{\rm tl}$, the system does not show steady-state motion. Thus, in the following we assume $\Lambda_{\rm tl}$, $\Lambda_{\rm qp} > 5$.

The volume change rate as a function of triple line and quadruple junction mobility (Fig. 14) suggests that for $\Lambda_{\rm tl}$, $\Lambda_{\rm qp} > 100$ the drag effect is practically constant. However, for the intermediate regime ($5 < \Lambda_{\rm tl}$, $\Lambda_{\rm qp} < 100$) the triple lines seem to drag boundary motion more effectively than quadruple junctions as reflected by a much lower volume change rate for $\Lambda_{\rm tl} = \Lambda_{\rm qp}$.

For intermediate values of $\Lambda_{\rm tl}$, $\Lambda_{\rm qp}$ the differences in $\dot{V}(\Lambda)$ are markedly pronounced, because $\dot{V}(\Lambda)$ is more sensible to a change of $\Lambda_{\rm tl}$ than of $\Lambda_{\rm qp}$. The derivatives of the volume change rate with respect to $\Lambda_{\rm tl}$ and $\Lambda_{\rm qp}$ reveal that $\left(\mathrm{d}\dot{V}/\mathrm{d}\Lambda_{\rm tl}\right)_{\Lambda_{\rm qp}\to\infty}$ increases faster with decreasing $\Lambda_{\rm tl}$ than $\left(\mathrm{d}\dot{V}/\mathrm{d}\Lambda_{\rm qp}\right)_{\Lambda_{tj}\to\infty}$ with decreasing $\Lambda_{\rm qp}$ (Fig. 15). In essence, triple lines drag grain-boundary motion more effectively than quadruple junctions contrary to predictions of other authors [9].

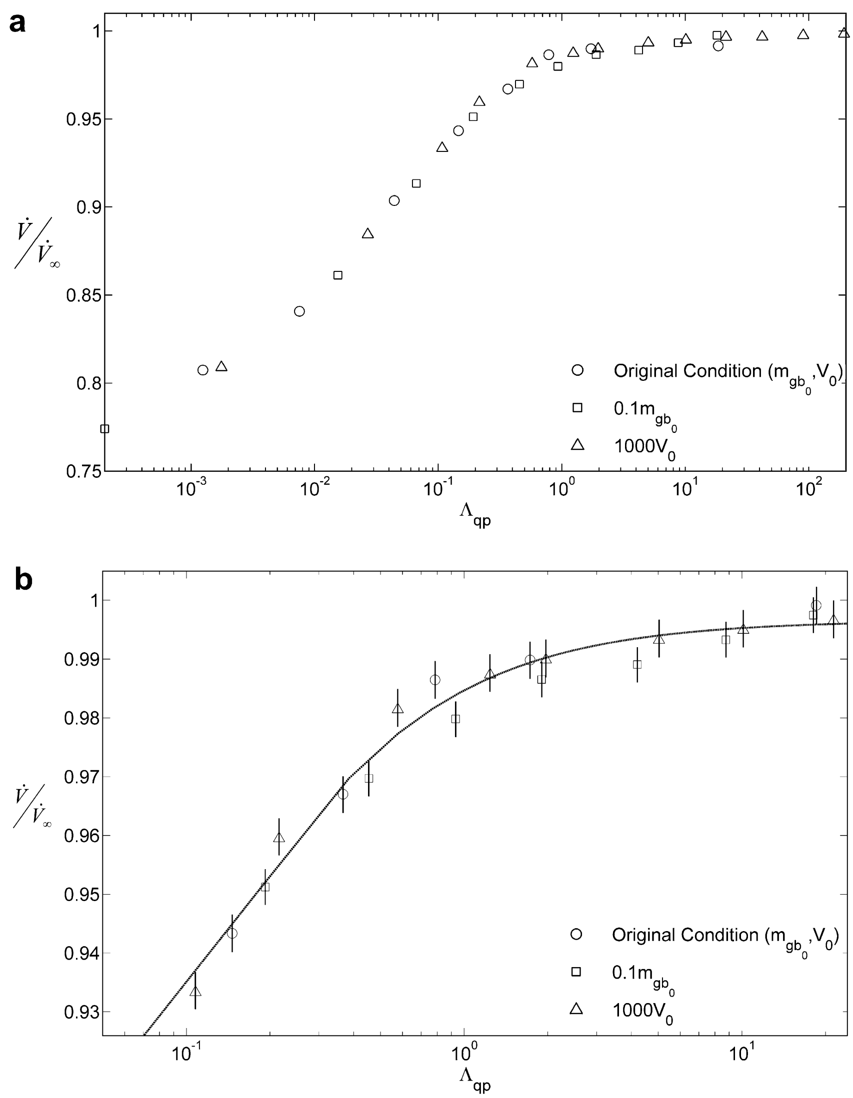

Fig. 12. Relative volume change rate as a function of Λ_{qp}. Three different conditions are shown: (○) original condition; (□) grain-boundary mobility reduced by a factor 10, and (Δ) the grain volume increased by a factor 1000; (b) magnification of Fig. 12a for low and medium values of Λ_{qp}, where the solid line is just a guide to the eye.

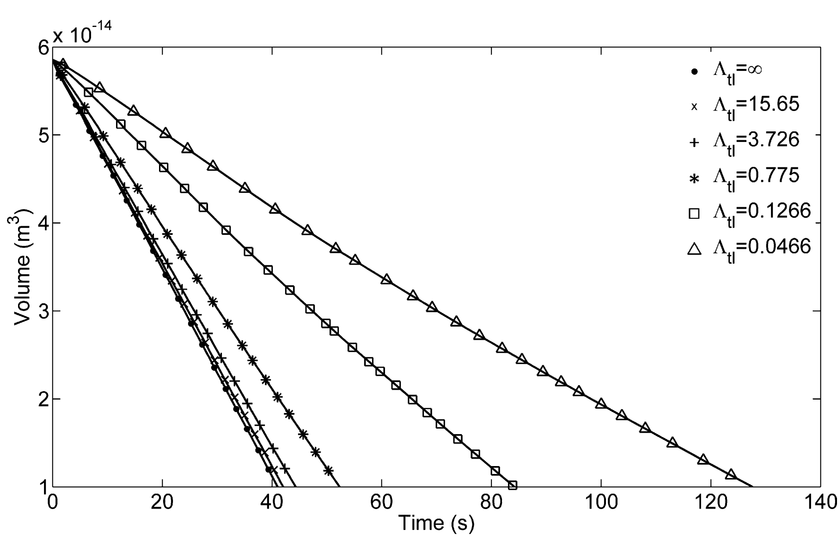

Fig. 13. Grain volume as a function of time for different values of Λ_{tl} (symbols are introduced along the lines for better identification).

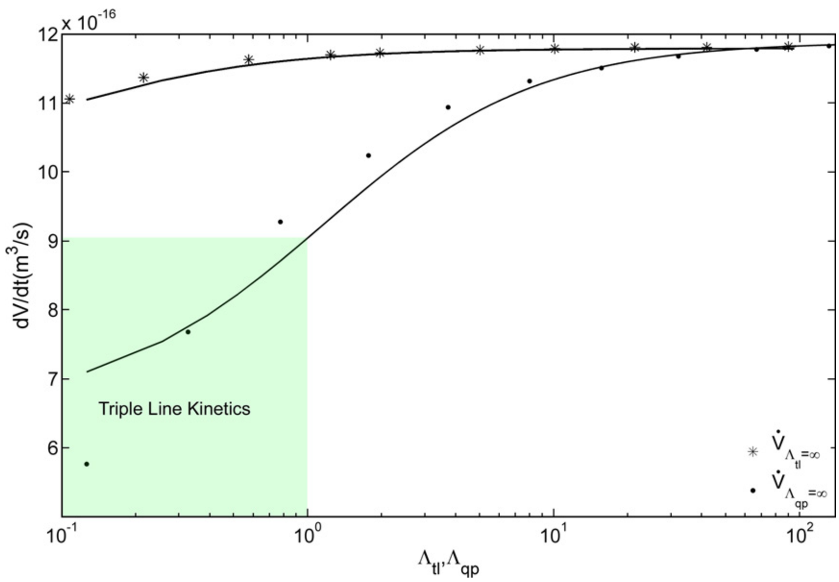

Fig. 14. Volume change rate, for (∗) Λ_{qp} is varied while Λ_{tl} is held infinite and for (●) Λ_{tl} is varied whereas Λ_{qp} is held infinite. The solid lines in this figure were obtained by fitting the simulation data to functions of the type $\dot{V} = A_h \cdot v(\Lambda_{qp})$ and $\dot{V} = A_h \cdot v(\Lambda_{tl})$, where A_h is the area of the hexagonal grain-boundary of the configuration in Fig. 4, and v is the displacement velocity of the same grain-boundary in dependency of Λ_{qp} and Λ_{tl}, respectively. The velocities can be determined with the combination of Eqs. (12) and (26), for the case of Λ_{qp}. For the case of Λ_{tl} see [4], where similar expressions can be found.

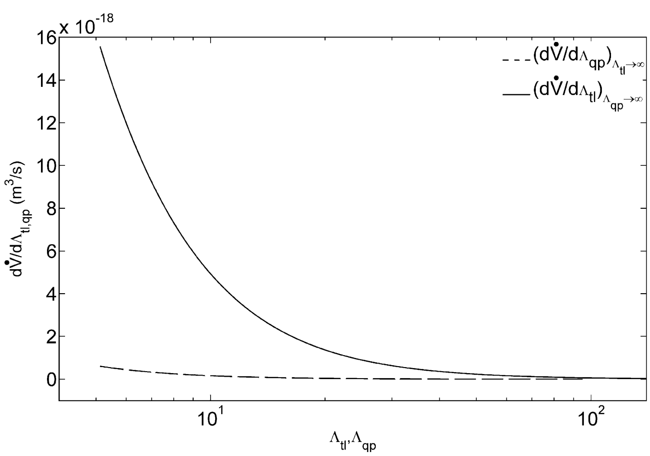

Fig. 15. The rate $\frac{d\dot{V}}{d\Lambda_i}$ $(i = \mathrm{tl}, \mathrm{qp})$ as a function of Λ_i. These curves were obtained by numeric differentiation of the curves in Fig. 14.

6. Comparison with theoretical predictions

6.1. Analytical description of the volume rate of change

The von Neumann–Mullins relation gives a general and physically transparent description of the growth of a definite grain in a polycrystal. The main advantage of this relation is its precise topological nature: a grain with topological class $n > 6$ will grow while grains with $n < 6$ will shrink. All attempts to derive a three-dimensional analog [10–12] were successful only to a certain extent.

Recently, MacPherson and Srolovitz [13] introduced the n-dimensional equivalent to the von Neumann–Mullins law. The MacPherson–Srolovitz relation (Eq. (16)) considers two terms, the mean width $L(D)$ of a given domain D (grain) and the length of the edges $e(D)$ (triple lines) of the same domain.

$$\frac{dV}{dt} = -2\pi m_{gb}\gamma\left(L(D) - \frac{1}{6}e(D)\right) \tag{16}$$

where dV/dt is the volume change rate of the domain, m_{gb} is the grain-boundary mobility and γ is the grain-boundary energy. $L(D)$ and $e(D)$ are defined as follows:

$$L(D) = \frac{1}{2\pi}\sum_{i}^{n_{ef}} \beta_i e_i \tag{17}$$

$$e(D) = \sum_{i}^{n_{tl}} e_i^{tl} \tag{18}$$

The term $e(D)$ is simply the length of the triple lines of a given grain and is equal to the sum of the length of all triple lines n_{tl} of such grain. In turn, the term $L(D)$ reflects the local variation of the surface with respect to a fixed reference. The normal to each element dS of the surface characterizes its spatial orientation, which may be different from the orientation of other elements surrounding dS. Its difference to an adjacent element across a junction of length e_i is denoted by the angle β, also known as the turning angle. The sum over all junctions n_{ef} leads to the mean width of the whole domain. In particular, the orientation difference β across a triple line corresponds to the external dihedral angle as established by the surface tensions of the adjoining grain boundaries. Another interesting feature of this term is that it introduces implicitly the curvature of the surface. In the following, we will compare the simulation results with the MacPherson–Srolovitz equation for the case when

$\Lambda_{\rm tl} = \infty$ and $\Lambda_{\rm qp} = \infty$ and subsequently, the effect of low values of these parameters on the same equation.

6.2. Comparison of simulation results with the MacPherson–Srolovitz equation

The special configuration which was introduced in Section 4 of this paper makes it possible to determine analytically all the terms of Eq. (16). In Fig. 16, one grain of the configuration is shown. Two new variables, a and d, define the dimensions of the grain; d is the length of the longitudinal triple lines while a is the length of the triple lines of the hexagonal cross section. The curvature of the triple line is included in a.

The term $e(D)$ for this grain reads

$$e(D) = \sum_{i}^{n_{\rm tl}} e_i^{\rm tl} = 6d + 12a \tag{19}$$

and the term $L(D)$ is given by

$$L(D) = \frac{1}{2\pi}\sum_{i}^{n_{ef}} \beta_i e_i = \frac{1}{2\pi}\left(2L_k + \frac{1}{3}\pi \cdot 6d + \frac{1}{3}\pi \cdot 12a\right) = \frac{L_k}{\pi} + d + 2a \tag{20}$$

where L_k is the unknown mean width of the two curved faces of the grain. Because all other grain boundaries are flat, $\beta = 0$ and thus, their surfaces does not contribute to the mean width.

Combining Eqs. (19) and (20) with Eq. (16) the volume change rate can be determined

$$\frac{dV}{dt} = -2\pi m_{\rm gb}\gamma\left(\frac{L_k}{\pi} + d + 2a - d - 2a\right) = -2m_{\rm gb}\gamma L_k \tag{21}$$

The volume change rate for the considered configuration depends exclusively on the term L_k which represents the only curved grain boundaries in the configuration. Since the configuration moves in steady-state, $\dot{V} = \text{const}$. This prediction was examined by computer simulations. The three-dimensional vertex simulations rendered independently the parameters needed for the MacPherson–Srolovitz relation [13] and $\dot{V}$.

Fig. 17 shows the calculated parameters $L(D)$ and $e(D)$ taken directly from the geometry of the considered grain. If the grain evolves in steady-state the curves $L(D,\text{t})$ and $e(D,t)$ have to be parallel to yield $\dot{V} = \text{const.}$ in Eq. (16).

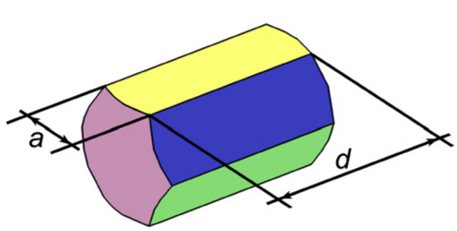

Fig. 16. One grain of the special grain assembly and the dimensions a and d.

According to Fig. 17, this condition is evidently fulfilled. In addition, the value of the volume change rate calculated according to Eq. (14) agrees perfectly with the simulation results (Fig. 18). The observed small deviation is attributed to the calculation of the parameter $L(D)$ which is very sensitive to the size of the mesh.

Another important question is whether the MacPherson–Srolovitz relation holds for the general case when the driving force is not constant (i.e. the curvature depends on time). We can use the configuration shown in Fig. 2 to investigate the problem. As demonstrated in Section 3, this configuration does not evolve in steady-state. Correspondingly, the volume does not change linearly with time i.e. $\dot{V}$ is not constant (Fig. 19).

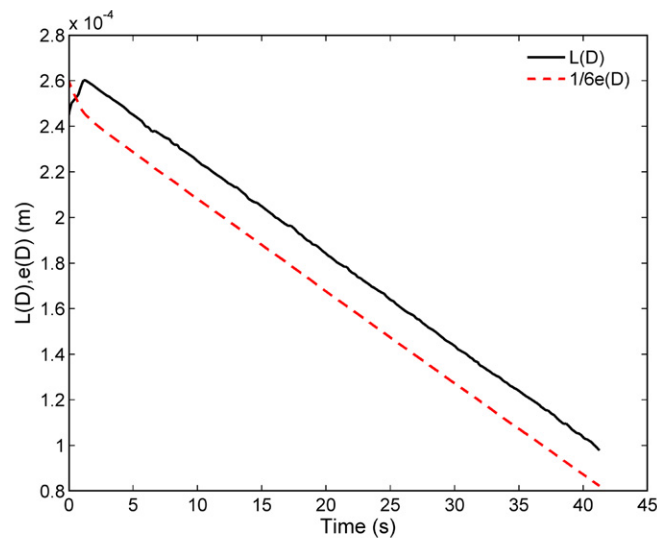

Fig. 17. The temporal evolution of the parameters $L(D)$ and $e(D)$.

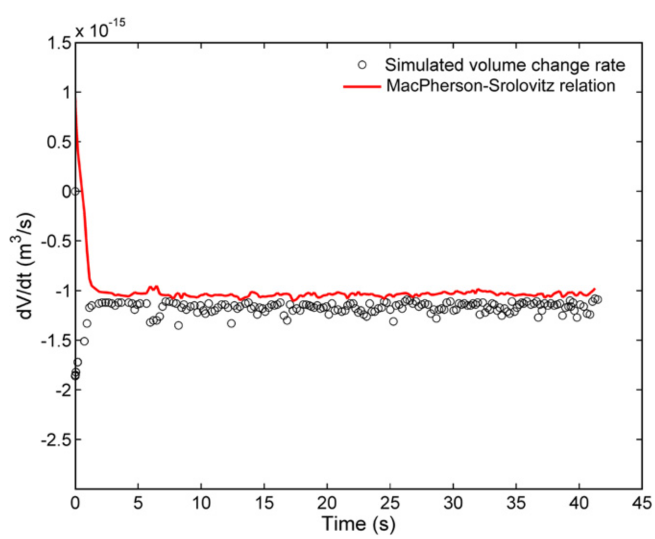

Fig. 18. Comparison of dV/dt as obtained from simulations and calculated using Eq. (16) for $\Lambda_{\rm qp} = \Lambda_{\rm tl} = \infty$.

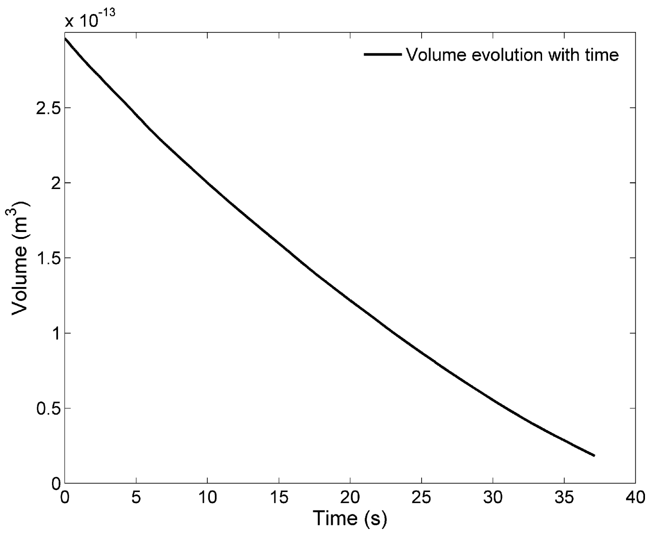

Fig. 19. Simulated temporal evolution of the grain in Fig. 1.

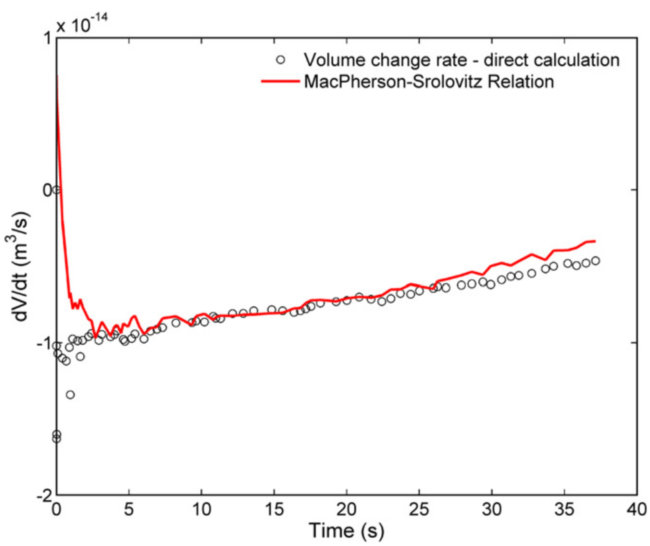

Fig. 20. Comparison of theoretical predictions (Eq. (16)) and simulation results for $\Lambda_{\mathrm{qp}} = \Lambda_{\mathrm{tl}} = \infty$.

According to Fig. 20, the predictions of Eq. (16) agree very well with the volume change rate calculated from the data of Fig. 19. For long times, simulations and theory seem to diverge. However, this is caused by the decreasing number of triangular facets in the simulation as the grain shrinks which increases the error in the calculation of $L(D)$.

6.3. The effect of a finite quadruple junction and triple line mobility on the MacPherson–Srolovitz equation

For the derivation of Eq. (16), MacPherson and Srolovitz considered that the dihedral angle at triple lines attains its equilibrium value of 120°. Consequently, the angle between triple lines at quadruple junctions must reach a value of ~109.47°. Since a finite (low) mobility of these elements influences the value of these equilibrium angles, it is expected that the MacPherson–Srolovitz equation fails to predict adequately the volume change rate of a domain in case of a limited mobility of the domain's junctions. To verify this, several simulations with the configuration sketched in Fig. 4 were performed with different (non-infinite) values of triple line and quadruple junction mobility. In all cases, a deviation of Eq. (16) from the simulation results was observed. However, for a finite quadruple junction mobility, the effect was less pronounced than for a finite triple line mobility. With the purpose to demonstrate this point, the simulations results for $\Lambda_{\mathrm{tl}} = 0.12$ are compared with the predictions of Eq. (16) in Fig. 21, which shows a marked discrepancy.

One major effect of a finite quadruple junction mobility is a change of the curvature of the triple lines, which implicitly alters also the length of the triple lines. The total length of the triple lines $e(D)$ for the configuration shown in Fig. 16 is given by the sum of all triple line lengths a and d. If the longitudinal triple lines are straight the calculation of d is very simple, however, the determination of the length a becomes problematic because the triple lines of the hexagonal cross section are now curved. However, Eq. (11) describes the shape of the triple line and can be used to calculate the triple line length. The length l of any two-dimensional curve of the form $y = f(x)$ in the interval $[s_1, s_2]$ is given by

$$l = \int_{s_1}^{s_2} \sqrt{1 + \left(\frac{\mathrm{d}y}{\mathrm{d}x}\right)^2}\,\mathrm{d}x \tag{22}$$

Applied to Eq. (11) we obtain

$$l = \int_0^{x_0} \sqrt{1 + \frac{\mathrm{e}^{2x/c}}{1 - \mathrm{e}^{2x/c}}}\,\mathrm{d}x = \int_0^{x_0} \frac{\mathrm{d}x}{\sqrt{1 - \mathrm{e}^{2x/c}}} \tag{23}$$

where $c = x_0/\ln \sin \alpha$. Integration leads to

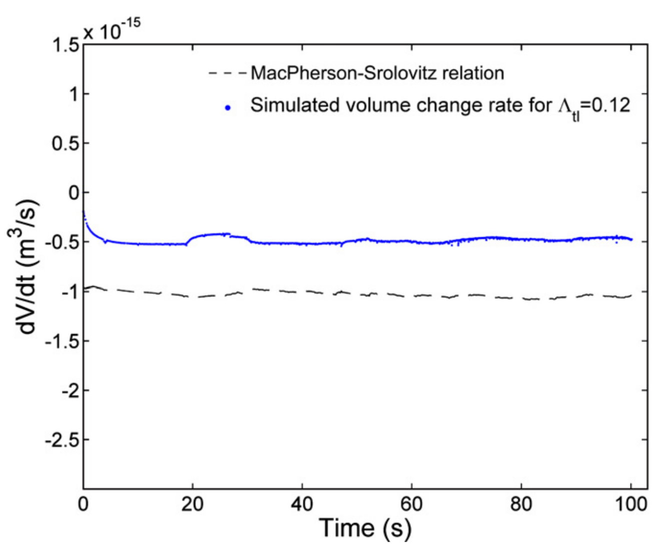

Fig. 21. A comparison of the MacPherson–Srolovitz equation with the simulations results for the case of a finite triple line mobility reveals a strong discrepancy.

$$l = \frac{x_0}{\ln \sin \alpha} \operatorname{arcsech} \sin \alpha = \frac{x_0}{\ln \sin \theta} \ln \left(\frac{1 + \sqrt{1 - \sin^2 \theta}}{\sin \theta} \right) \tag{24}$$

Accordingly, the length of the triple lines of the hexagonal cross section can be easily calculated as

$$a = 2l = \frac{2x_0}{\ln \sin \theta} \ln \left(\frac{1 + \cos \theta}{\sin \theta} \right) \tag{25}$$

By series expansion of Eq. (15), we find the angle θ as a function of Λ_{qp}

$$\theta = \frac{2\Lambda_{qp}}{3\Lambda_{qp} + \sqrt{\Lambda_{qp}(9\Lambda_{qp} + 2)}} + \frac{\pi}{2} \tag{26}$$

While the length a strongly depends on Λ_{qp}, the term d does not, at least not directly. Actually d changes linearly with time

$$d = d_0 - 2v_{gb}t \tag{27}$$

where d_0 is the length of the longitudinal triple line at $t = 0$, v_{gb} is the velocity of the front and rear faces of the grain. This velocity depends naturally on Λ_{qp} but remains constant for $\Lambda_{qp} = \text{const}$. From the simulation, it is possible to extract the dependency of the parameter a on Λ_{qp} and to test the validity of the derived equations. For this, the length a/x_0 from the simulations is compared with Eq. (25) (Fig. 22).

It would be also desirable to know analytically the dependency of $L(D)$ on θ and Λ_{qp}. However, for the solution of this problem, the velocity of the grain-boundary needs to be related to the velocity of the triple lines, in a similar way as the triple line velocity relates to the quadruple junction velocity. This would introduce the ratio of grain-boundary and triple line energies, which is so far unknown.

Nevertheless, from the simulations this dependency can be extracted. According to the definition of $L(D)$, the flat grain boundaries do not contribute to this term. Moreover, the turning angle of the longitudinal triple lines does not depend on Λ_{qp}. Only the curved grain boundaries and the turning angle of the triple lines at the cross-section vary with changing Λ_{qp}. In Fig. 23, $L(D)$ for the curved grain boundaries is shown as a function of Λ_{qp}. $L(D)$ increases rapidly for small $\Lambda_{qp} < 1$. In the intermediate range ($1 < \Lambda_{qp} < 20$), a transition occurs to a constant value of $L(D)$, which correspond to the curvature of the grain-boundary at zero drag force.

Since the parameters $L(D)$ and $e(D)$ are affected by a finite quadruple junction mobility, it can be expected that a modified MacPherson–Srolovitz relation exists that takes the additional parameter Λ_{qp} into account like recently shown for the modification of the von Neumann–Mullins relation for a limited triple junction mobility in two-dimensional grain growth [5,14]. Since both $L(D)$ and $e(D)$ are expected to depend on the junction mobility, a generalized MacPherson–Srolovitz relation will be of the form

$$\frac{dV}{dt} = f(L(\Lambda_{qp}, \Lambda_{tl}), e(\Lambda_{qp}, \Lambda_{tl})) \tag{28}$$

7. Summary

The effect of a finite quadruple junction mobility on grain microstructure evolution was studied. Based on a special grain assembly we introduced the parameter Λ_{qp} which describes the influence of the quadruple junction mobility on grain-boundary motion. By computer simulation using a there-dimensional vertex model, it was demonstrated that such configuration evolves in steady-state. The simulation results also showed excellent agreement with the predictions of the MacPherson–Srolovitz relation. It was

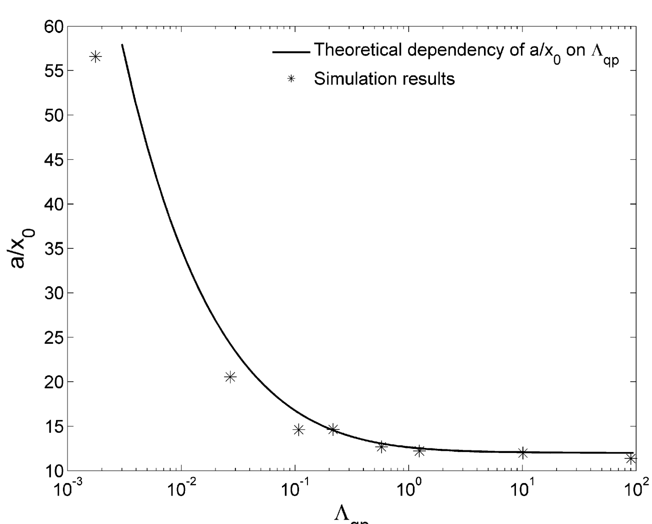

Fig. 22. Dependency of the triple line length on the parameter Λ_{qp}.

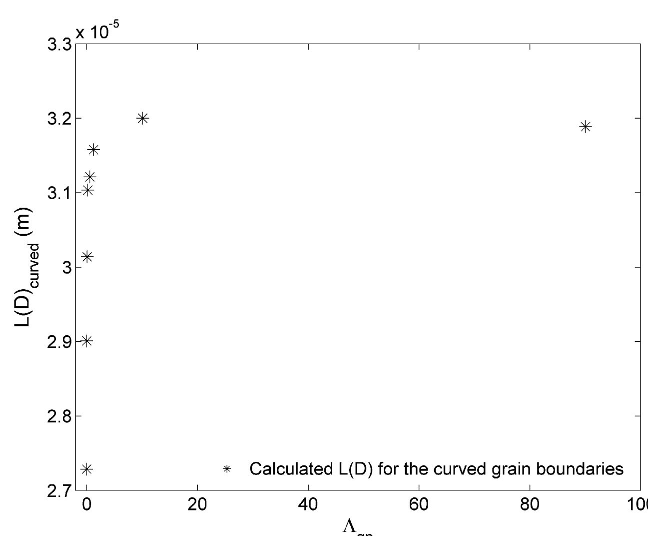

Fig. 23. Dependency of $L(D)$ on Λ_{qp} for the curved grain boundaries of the special grain assembly shown in Fig. 4.

found that quadruple junctions can affect the kinetics of grain growth; the growth rate was reduced with a decrease of junction mobility. The effect of a finite quadruple junction mobility on the MacPherson–Srolovitz relation was determined.

Acknowledgements

Financial assistance from the Deutsche Forschungsgemeinschaft (DFG MO 848/7-1) is gratefully acknowledged. The cooperation was supported by the Deutsche Forschungsgemeinschaft (DFG Grant 436 RUS 113/714/0-1(R)) and the Russian Foundation of Fundamental Research (Grant DFG-RRFI 05-02-04017). L.A. Barrales-Mora conveys his thanks to the Deutscher Akademischer Austauschdienst (DAAD) and the Secretary of Public Education (SEP) of Mexico for respective PhD stipends.

Appendix A. Three-dimensional vertex model

For the simulations, a three-dimensional vertex model that considers a front tracking approach was utilized. In such approach, only the grain boundaries are discretized whereas the grain interior is not. The grains are considered only as the volume enclosed by grain boundaries and maintain their crystallographic orientation. The boundaries (internal surfaces) are discretized in triangular facets (Fig. A.1a). The facet construction of the grain boundaries follows a similar procedure as outlined in Ref. [15]. For the vertices of these facets, the forces and velocities are calculated from the local geometry [16]. The forces at vertices arise from the surface tensions of the triangular facets that adjoin the respective vertex.

Fig. A.1b shows a vertex and the facets surrounding it. The force F_{f1} due to the shaded facet f_1 on the vertex P_0 is given by

$$\vec{F}_{f_1} = \frac{\gamma}{2} \cdot \frac{\vec{s}_0 \times (\vec{s}_1 \times \vec{s}_0)}{\|\vec{s}_1 \times \vec{s}_0\|}. \tag{A1}$$

where γ is the grain-boundary energy, and $\vec{s}_0, \vec{s}_1, \vec{s}_2$ are the edge vectors in the facet, which are fully determined by the position of the vertices (P_0, P_1 and P_2) conforming the facet (Fig. A.1b).

The sum of the forces over all facets surrounding the vertex leads to the net force

$$\vec{F}_{\text{sum}} = \frac{\gamma}{2} \cdot \sum_{i=1}^{n} \frac{\vec{s}_{0i} \times (\vec{s}_{1i} \times \vec{s}_{0i})}{\|\vec{s}_{1i} \times \vec{s}_{0i}\|}. \tag{A2}$$

where n is the total number of facets meeting at P_0. The velocity of the vertex reads

$$\vec{v} = m_{\text{eff}} \cdot \vec{F}_{\text{sum}} = \frac{1}{D_{\text{f}}} \cdot \vec{F}_{\text{sum}} \tag{A3}$$

where m_{eff} is the effective mobility of the vertex and D_{f} is the drag factor, which is defined as

$$D_{\text{f}} = \frac{A_n}{m_{\text{gb}}} + \frac{\mathrm{d}s}{m_{\text{tl}}} + \frac{1}{m_{\text{qp}}}. \tag{A4}$$

m_{gb}, m_{tl}, and m_{qp} are the grain-boundary, triple line and quadruple junction mobilities, respectively, ds is the mean distance between adjacent vertices over a triple line, and A_n is the projected area of the surrounding facets onto the direction of motion.

The discretization of the internal surfaces in triangular facets permits also the calculation of the turning angle β of the grain boundaries (Eq. (17)) by simple vector operations between facets adjacent to an edge. The angular change of the surface of a boundary is given by the angle between normal vectors of adjacent facets to an edge. For instance, according to the geometry depicted in Fig. A.1b, the normal vectors $\vec{n}_1$ and $\vec{n}_2$ to the facets f_1 and f_2 in Fig. A.1b can be respectively defined as

$$\vec{n}_1 = \frac{s_1 \times s_0}{\|s_1 \times s_0\|} \tag{A5}$$

and

$$\vec{n}_2 = \frac{s_2 \times s_3}{\|s_2 \times s_3\|} \tag{A6}$$

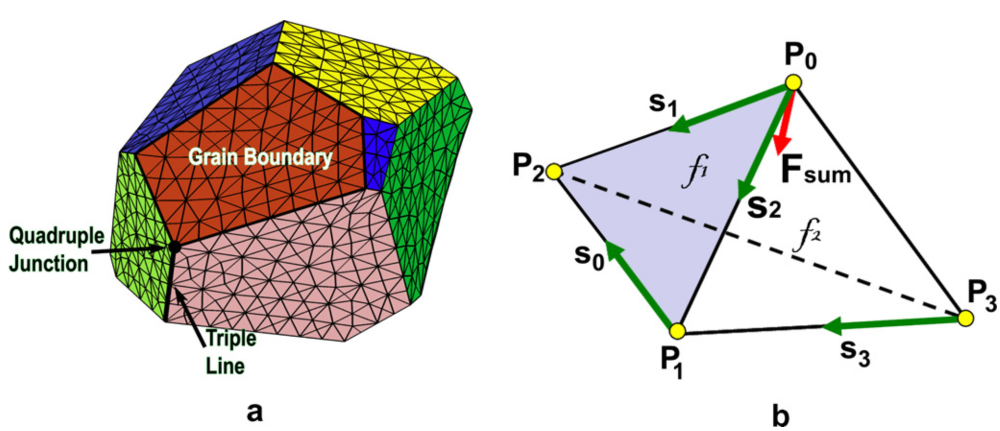

Fig. A.1. (a) Three-dimensional grain with grain boundaries discretized in triangular facets. Different structural elements are distinguished; (b) the forces at triple junctions result from the surface tensions of the attached facets.

The turning angle β_{ff} between these two facets is obtained simply by the dot product of the normal vectors as follows:

$$\beta_{\mathrm{ff}} = \arccos(\vec{n}_1 \cdot \vec{n}_2) \tag{A7}$$

References

[1] Gottstein G, Shvindlerman LS. Scripta Mater 2006;54:1065.
[2] Ivanov VA, Molodov DA, Shvindlerman LS, Gottstein G. Acta Mater 2004;52:969.
[3] Protasova SG, Gottstein G, Molodov DA, Sursaeva VG, Shvindlerman LS. Acta Mater 2001;49:2519.
[4] Czubayko U, Sursaeva VG, Gottstein G, Shvindlerman LS. Acta Mater 1998;46:5863.
[5] Gottstein G, Ma Y, Shvindlerman LS. Acta Mater 2005;53:1535.
[6] Gottstein G, Shvindlerman LS. Scripta Mater 2005;52:863.
[7] Galina AV, Fradkov VE, Shvindlerman LS. Phys Met Metallogr 1987;63:165.
[8] Mullins WW. J Appl Phys 1956;27:900.
[9] Bréchet Y, Militzer M. Scripta Mater 2005;52:1299.
[10] Hilgenfeldt S, Krynik AM, Koehler SS, Stone HA. Phys Rev Lett 2001;86:2685.
[11] Glicksman ME. Phil Mag 2005;85:3.
[12] Rios PR, Glicksman ME. Acta Mater 2007;55:1565.
[13] MacPherson RD, Srolovitz DJ. Nature 2007;446:1053.
[14] Gottstein G, Shvindlerman LS. Scripta Mater 1998;10:1541.
[15] Brakke KA. Exp Math 1992;1:141.
[16] Barrales Mora LA, Shvindlerman LS, Mohles V, Gottstein G. Mater Sci Forum 2007;558:1051.